Biophysical Journal
Article

Biophysical Society

MAS ^{1}H NMR Probes Freezing Point Depression of Water and Liquid-Gel Phase Transitions in Liposomes

Abhishek Mandal[1] and Patrick C. A. van der Wel[1,*]
[1]Department of Structural Biology, University of Pittsburgh School of Medicine, Pittsburgh, Pennsylvania

ABSTRACT The lipid bilayer typical of hydrated biological membranes is characterized by a liquid-crystalline, highly dynamic state. Upon cooling or dehydration, these membranes undergo a cooperative transition to a rigidified, more-ordered, gel phase. This characteristic phase transition is of significant biological and biophysical interest, for instance in studies of freezing-tolerant organisms. Magic-angle-spinning (MAS) solid-state NMR (ssNMR) spectroscopy allows for the detection and characterization of the phase transitions over a wide temperature range. In this study we employ MAS ^{1}H NMR to probe the phase transitions of both solvent molecules and different hydrated phospholipids, including tetraoleoyl cardiolipin (TOCL) and several phosphatidylcholine lipid species. The employed MAS NMR sample conditions cause a previously noted substantial reduction in the freezing point of the solvent phase. The effect on the solvent is caused by confinement of the aqueous solvent in the small and densely packed MAS NMR samples. In this study we report and examine how the freezing point depression also impacts the lipid phase transition, causing a ssNMR-observed reduction in the lipids' melting temperature (T_m). The molecular underpinnings of this phenomenon are discussed and compared with previous studies of membrane-associated water phases and the impact of membrane-protective cryoprotectants.

INTRODUCTION

Integral membrane proteins are essential for many cellular functions and represent important drug targets. The ability of membrane-embedded proteins to perform their biological activity is frequently influenced by, and even dependent on, the structure, dynamics, and physical properties of the surrounding lipid bilayer (1–4). Moreover, critical biological processes such as membrane fusion and fission require the modulation of physical and structural properties of the membrane. To probe the molecular underpinnings of these processes, there has been an ongoing effort to understand the fundamental character of lipid bilayers, based in large part on the study of membrane-mimicking lipid vesicles (5). Under biologically relevant conditions, biomembranes feature a lipid bilayer that is in a liquid crystalline, highly dynamic, state. Upon changing of conditions, lipid membranes can experience cooperative phase transitions between fluid and gel-like phases, and between bilayer and nonbilayer assemblies. These phase transitions occur in response to changes in the level of hydration, temperature, and membrane composition. There is much interest in these phenomena, for instance, in context of the protective mechanisms employed by drought- and freezing-tolerant organisms (6). An improved understanding of the impact of solvent and lipid freezing on the structure of membranes is also important for structural biology methods that employ low temperature conditions to study lipid-bilayer-embedded proteins.

Both low temperature and sample dehydration can lead to a lipid or lipid mixture undergoing a transition from the liquid crystalline (L_α) to the gel state. The transition temperature between the L_α and gel phase is known as the melting temperature (T_m). This kind of phase transition has important biological consequences, affecting both the barrier function of the membrane and the structure and function of membrane-associated proteins. Thus, it is not surprising that organisms and cells modulate their membranes' acyl chain composition in response to changes in, e.g., growth temperature (7–9). It is also known that membrane-interacting proteins and peptides modify the phase behavior of their lipid membrane environment (10,11).

Given the above, there has been a long-standing interest in studying the molecular underpinnings of lipid structure, dynamics, and phase behavior. Depending on their chemical structure, different lipids can have dramatically different transition temperatures. Although a lipid's T_m depends on both the type of lipid head group and the identity of the attached acyl chains (Fig. 1), it is well-established that the acyl chains have

Submitted April 27, 2016, and accepted for publication September 21, 2016.
*Correspondence: vanderwel@pitt.edu
Editor: Mei Hong
http://dx.doi.org/10.1016/j.bpj.2016.09.027

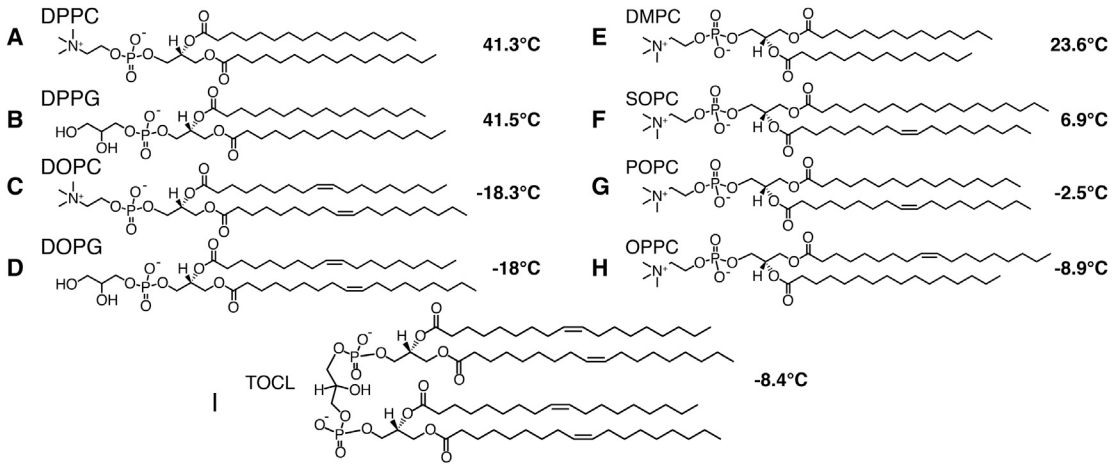

FIGURE 1 Phospholipid species and their gel-to-liquid crystalline phase transition temperatures (T_m): (*A*) DPPC, (*B*) DPPG, (*C*) DOPC, (*D*) DOPG, (*E*) DMPC, (*F*) SOPC, (*G*) POPC, (*H*) OPPC, and (*I*) TOCL. The corresponding T_m value is indicated alongside each lipid species, based on literature reports (13,14) and DSC (Fig. S1).

a particularly prominent effect (12,13). Despite having different headgroups (in both charge and size), 1,2-dipalmitoyl-*sn*-glycero-3-phosphocholine (DPPC) and 1,2-dipalmitoyl-*sn*-glycero-3-phosphoglycerol (DPPG) have similar T_m values of 41.3°C and 41.5°C, respectively (Fig. 1, *A* and *B*) (13,14). In comparison, the monounsaturated variants, DOPC and DOPG, have T_m values of −18.3°C and −18°C, respectively (Fig. 1, *C* and *D*). Thus, the T_m of a lipid bilayer strongly correlates to the acyl chain structure (12). These data also illustrate the general observation that the introduction of double bonds cause increased disorder and thus lowers the T_m. Thus, the gel transition reflects an event that predominantly involves the acyl chains, and appears to be decoupled from the headgroup and solvent motion. The apparent independence of solvent and acyl chain dynamics can also be appreciated from the abovementioned DOPC and DOPG T_m values, which are well below water's freezing point.

These insights are derived from numerous studies reporting transition temperatures based on a variety of techniques, including x-ray methods, calorimetry, and nuclear magnetic resonance (NMR). Among these methods, the use of solid-state NMR (ssNMR) is based on its ability to detect changes in the site-specific dynamics of lipids, which undergo dramatic changes at the transition temperatures (15–17). The ssNMR measurements of order parameters and relaxation rates provide direct insight into the dynamics of individual chemical groups along the lipid acyl chains and head groups. Classical ssNMR studies took advantage of the ability of ^{31}P NMR to probe the dynamics of the lipid headgroups and thus detect the phase transitions (18). ^{2}H NMR on lipids with deuterated acyl chains allows the extraction of site-specific order parameters, within the hydrophobic core of the lipid bilayer. More recent ssNMR studies of membranes increasingly employ magic-angle spinning (MAS) to permit the observation of individual ^{13}C and ^{1}H lipid sites, without isotopic labeling (19–23). Another benefit of MAS-based ssNMR is that it also provides powerful tools to study proteins associated with the membrane (24,25). This allows unique opportunities to probe how membrane dynamics and phase behavior affect the structure and dynamics of membrane-bound proteins (26–29).

We recently reported on our MAS ssNMR studies of peripherally membrane-bound cytochrome c (29), in which we observed the correlated dynamics of lipids and lipid-bound protein, in line with earlier studies (26,27). In the course of that work we also noted a surprising degree of apparent correlation between the dynamics of the hydrophobic core of the membrane and the dynamic properties of the bulk solvent. Here, we provide an in-depth and systematic examination of this phenomenon, through the use of MAS NMR spectroscopy. We show a consistent impact on the T_m of a variety of hydrated lipids, in absence of protein. The observed phase transition behavior furthers our understanding of lipid bilayer dynamics and phase behavior, with associated implications for our understanding of membrane cryoprotection in biology and in low-temperature structural biology of whole cells and membrane proteins.

MATERIALS AND METHODS

Materials

Purified 1,2-dioleoyl-*sn*-glycero-3-phosphocholine (DOPC), 1,2-dimyristoyl-*sn*-glycero-3-phosphocholine (DMPC), 1-stearoyl-2-oleoyl-*sn*-glycero-3-phosphocholine (SOPC), 1-palmitoyl-2-oleoyl-*sn*-glycero-3-phosphocholine (POPC), 1-oleoyl-2-palmitoyl-*sn*-glycero-3-phosphocholine (OPPC), and 1',3'-bis[1,2-dioleoyl-*sn*-glycero-3-phospho]-*sn*-glycerol (TOCL) lipids were obtained from Avanti Polar Lipids (Alabaster, Alabama). The lipid structures are shown in Fig. 1.

Sample preparation

Stock solutions containing 10 mg of single or mixed lipids in chloroform were dried to a film under N_2 flow and left under vacuum overnight to

remove trace solvents. The lipid film was resuspended by adding 1 mL of Milli-Q H_2O and shaking gently for 15 min on a tabletop shaker at room temperature. In the case of lipids with a T_m close to room temperature, the sample was shaken at 32°C. Multilamellar vesicles (MLVs) were prepared by freeze-thawing the resuspended lipids five times as described before (29). A final sample volume of 35 μL each was packed for all lipid samples. To maintain a hydrated environment in the samples, lipid MLVs were pelleted directly into 3.2 mm NMR sample rotors using ultracentrifugation. Excess supernatant was removed after which the sample rotors were sealed before ssNMR measurements. The sample pelleting was done as described before (29–31), using a custom-built packing tool reminiscent of sedimentation devices (32). The packing process involved ultracentrifugation in a Beckman Coulter (Indianapolis, IN) L-100 XP centrifuge with a SW-32 Ti rotor for 1 h at 134,000 g. For most samples the packing was done at 4°C, except for DMPC that was packed at 30°C.

MAS ssNMR spectroscopy

MAS ssNMR experiments were performed on wide-bore 600 and 750 MHz spectrometers (Bruker Biospin, Billerica, MA), as indicated. The former system was used with a 3.2 mm MAS probe with a HCN "EFree" coil, whereas the latter employed a 3.2 mm HCN MAS probe. Unless indicated otherwise, the samples were studied at a MAS rate of 8.333 kHz. Spectra were obtained at specified MAS rates using direct ^{1}H detection at multiple temperature points across a wide temperature range. On the 750 MHz spectrometer, cooling and heating series of 1D spectra for DOPC/TOCL and DMPC samples were acquired at intervals of ~4°C between 22°C (49°C for DMPC) and −38°C sample temperatures. On the 600 MHz spectrometer the 1D spectra for POPC, OPPC, and SOPC were acquired at intervals of 7°C from 28°C down to −7°C, and then at intervals of 1.4°C from a sample temperature of −12°C to −40°C. The samples were allowed to equilibrate at each temperature for 15 min before a spectrum was acquired. Additional experimental details are specified in figure legends and in text. Temperature was regulated using cooled gas from a BCU-X or BCU II chiller units (Bruker Biospin). All reported temperatures reflect the internal sample temperature, as determined by a combination of external calibration and measurements on the sample itself. The external sample temperature calibrations were performed on a reference KBr sample under identical experimental conditions, in the form of ^{79}Br T_1 and chemical shift measurements (33,34). These measurements were complemented with an analysis of the ^{1}H shifts of unfrozen water and lipid methyl peaks, as previously reported (35,36). NMR spectra were processed using Bruker Topspin and NMRPipe software (37). Indirect referencing of the ^{1}H shifts relative to aqueous DSS (4,4-dimethyl-4-silapentane-1-sulfonic acid) was based on measurement of the adamantane ^{13}C chemical shift (29). Phase correction, baseline correction, and Fourier transformation were applied to all spectra. Exponential line broadening of 5 Hz was applied to all spectra acquired on the 600 MHz spectromter. Peak picking, peak intensity measurements, and plotting were done using CcpNmr Analysis program from the Collaborative Computation Project for the NMR community (CcpNmr) (38,39).

Differential scanning calorimetry

DSC measurements were performed on a PerkinElmer (Waltham, MA) Pyris 6 DSC instrument in the Materials Characterization Lab of the University of Pittsburgh. Lipid samples were prepared as discussed above. The hydrated MLVs were packed in a sealable sample pan (TA Instruments, New Castle, DE) and cold-welded to hermetically seal the sample. The DSC measurement started with an initial sample equilibration at −30°C for 10 min before ramping up the temperature to 20°C at a scan rate of 2°C/min. After a 10 min incubation at 20°C, a cooling run was performed at the same scan rate and then the entire procedure was repeated once more.

RESULTS

MAS NMR probing of solvents and lipid dynamics

We recently reported on our MAS ssNMR studies of TOCL/DOPC (1:4 molar ratio) large unilamellar vesicles (LUVs) in presence of 2.5 mol-% of membrane-bound cytochrome c (29). In variable temperature ^{1}H and ^{13}C MAS ssNMR measurements we detected the temperatures at which the solvent froze and the liquid-to-gel transition of the lipids occurred. In line with earlier MAS ssNMR studies (40–43), the aqueous solvent (20 mM HEPES buffer at pH 7.4) froze at temperatures significantly lower than 0°C. This effect stems from the reduced length scales of water pockets in the sample, compared with bulk water that freezes at 0°C (see Discussion). To our surprise, we also noted a substantial lowering of the lipid phase transition. To gain a better understanding of this unexpected observation, we pursued a series of systematic studies in absence of protein, which we report herein.

In analogy to our previous work (29), we probe the dynamics of the membrane and the solvent via ^{1}H MAS ssNMR measurements. At moderate MAS rates, as employed here, immobilized protons are strongly coupled to each other through ^{1}H-^{1}H dipolar interactions. These strong dipolar couplings lead to a large broadening of the ^{1}H signals in typical solid samples, which causes extensive peak overlap and a dramatic reduction in peak heights. This has led to (biomolecular) MAS ssNMR studies typically avoiding the detection of these ^{1}H signals, instead focusing on ^{13}C or ^{15}N detection. ^{1}H detection in liquid-state NMR experiments is not affected by this line-broadening effect, as the fast isotropic motion of molecules in solution cause motional averaging of the dipolar interactions. This averaging effect permits the detection of high-intensity, narrow peaks. Thus, only highly dynamic lipid and protein segments have narrow and intense ^{1}H signals in MAS NMR. The freezing of solvent and the liquid-to-gel lipid phase transition are detected as dramatic increases in ^{1}H line width and corresponding reductions in peak intensity (20–22).

Phase changes in monounsaturated mixed-lipid vesicles

First, we performed MAS ssNMR experiments on MLVs prepared from the same mixture of TOCL and DOPC, at a 1:4 molar ratio, as were used in our previous protein-bound vesicle studies (29). Thus, we test that the observed lowering of the solvent and water melting points was not due to the membrane-bound cytochrome c. The results of our 1D ^{1}H MAS NMR measurements on hydrated TOCL/DOPC MLVs are shown in Fig. 2. At room temperature (Fig. 2 *A*), the mobile water protons yield a sharp peak near 4.8 ppm. At this temperature, we also observe relatively narrow peaks for the lipids' methyl (CH_3) and

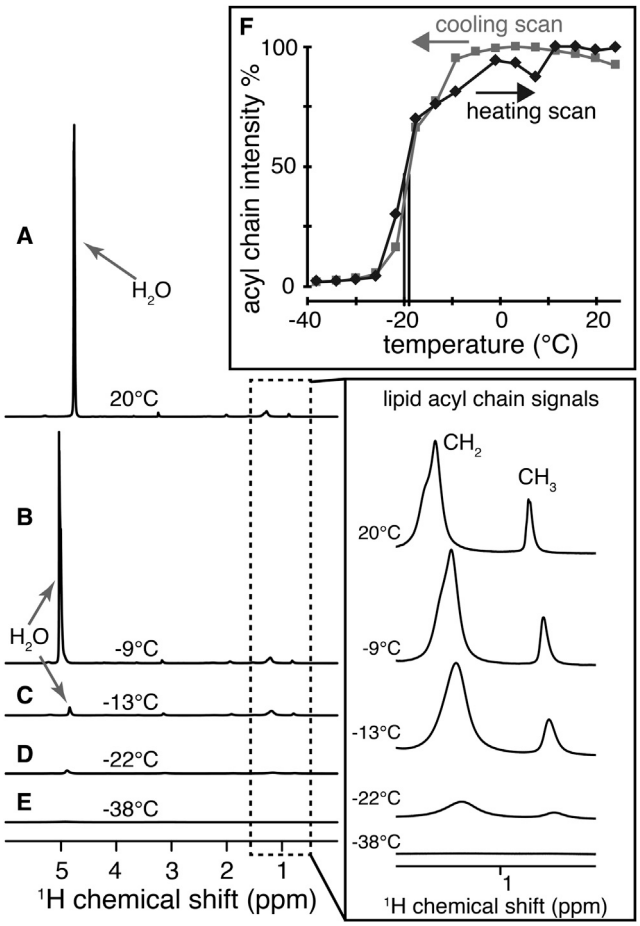

FIGURE 2 ^{1}H MAS ssNMR spectra of DOPC/TOCL MLVs at different sample temperatures. (*A*) At room temperature, narrow water (~4.8 ppm) and lipid CH_2 and CH_3 peaks indicate liquid-like motion. (*B*) At −9°C, peaks remain narrow and intense. (*C*) At −13°C, the water signal is attenuated due to ice formation, but lipid acyl chain signals remain intense. (*D*) At −22°C, the water peak has largely disappeared, and lipid peaks are partly attenuated because of the lipid phase transition. (*E*) At −38°C, all ^{1}H peaks are broadened beyond detection. The inset to the right shows enlarged versions of the lipid peaks. (*F*) Temperature-dependent peak heights for the acyl chain CH_2 peaks are shown.

methylene (CH_2) protons, showing up near 1 ppm (*see inset*). The CH_3 and CH_2 peak height and widths indicate that the lipid acyl chains are highly dynamic, consistent with the lipids forming a liquid crystalline bilayer phase (L_α) (20–22,29). As the temperature is decreased to −9°C (Fig. 2 *C*), the water peak moves (in accordance to the known temperature dependence of water ^{1}H shifts (35,36)), but remains intense and narrow. Thus, the water remains unfrozen even at −9°C. As is discussed in more detail below, this kind of solvent freezing point depression is typically seen for densely packed MAS ssNMR samples (29,42,43). Consistent with the T_m values of the DOPC and TOCL lipids, which are well below 0°C (Fig. 1), the lipid signals also remain narrow, indicating the persistence of the L_α phase (29). The T_m of hydrated TOCL was not previously reported, to the best of our knowledge, but was determined to be −8.4°C in DSC measurements shown in Fig. S1 in the Supporting Material. The peak intensities change notably at −13°C, when the intensity of the water peak dramatically decreases, indicating a freezing of most of the water in the sample (Fig. 2 *C*). However, a similar intensity change is not observed for the lipid protons (*inset*). These lipid proton signals remain intense until the sample is cooled to −22°C. Ultimately there is a complete loss of signal at the final temperature of −38°C (Fig. 2 *E*). The midpoint of the acyl chain dynamical transition was determined from the temperature-dependent acyl chain peak intensities to be at −20°C (Fig. 2 *F*). The acyl chain intensity changes were very similar in heating and cooling runs (Figs. 2 *F* and S2), with the cooling and heating transition points differing by a mere ~1°C. Thus, in these pure-lipid samples, we obtain a behavior of both the solvent and lipid dynamics that reproduces the data that we previously reported on DOPC/TOCL LUVs in presence of 2.5 mol-% of membrane-bound cytochrome c (29). The noted reduction in the lipid T_m is therefore not due to the effect of the membrane-bound protein.

Lipid and solvent freezing for single-lipid vesicles

Intrigued by these data, we performed analogous variable-temperature measurements on samples consisting of pure lipids with varying transition temperatures (Table 1). These single-lipid samples were chosen as they are well-characterized and have well-known T_m values determined by various different methods (12–14). The selected lipid types reflect a range of T_m values: near room temperature (DMPC), near water's normal freezing point (SOPC and POPC), and significantly below zero degrees Celsius (OPPC). The chemical structures and T_m values of the four lipid species are shown in Fig. 1, *E–H*, and Table 1. The fully saturated lipid DMPC has the highest T_m value, whereas the presence of double bonds in the monounsaturated lipids (SOPC, POPC, and OPPC) leads to lower T_m values.

Systematic series of ^{1}H MAS ssNMR spectra were obtained for each sample, with cooling runs starting at room temperature (or 49°C for DMPC) and cooling down to ~−38°C sample temperature. As noted above, measured cooling and heating runs were found to yield very similar transition points (Figs. 2, S2, and S3). As a function of temperature, we monitored the peak heights of the water and

TABLE 1 Phase Transition Temperatures

Species	Acyl Chains	$T_{m,Lit.}$ (°C)	$T_{m,MAS}$ (°C)	ΔT_m (°C)
DMPC	C14:0/C14:0	23.6	25	1.4
SOPC	C18:0/C18:1$_c$	6.9	−4	−11
POPC	C16:0/C18:1$_c$	−2.5	−14	−11
OPPC	C18:1$_c$/C18:0	−8.9	−19	−10

Literature T_m values from are from (13), the listed MAS ssNMR T_m values are from this study, and the final column (ΔT_m) lists the difference in T_m.

lipid methylene (CH_2) signals, in analogy to the data in Fig. 2. The obtained results are plotted in Fig. 3, *A–D*), for each sample, as indicated. In all four samples, the water signal (*blue diamonds*) retains a similar intensity down to well below the normal freezing point (*indicated with a vertical blue line at 0°C*). The freezing of water occurs around −20°C, as determined from the midpoint of the observed transition (*dashed blue vertical lines in* Fig. 3). We observe variations of a few degrees in the exact temperature at which water freezes in different samples, due to variability in the volume of the bulk water present in the samples.

We determined the lipids' phase transition via a similar analysis of the change in intensity of the CH_2 lipid signals. Fig. 3 shows these peak heights after normalization relative to the maximum peak intensity across the entire temperature range under study. Similar to the solvent, the lipid acyl chain signals show a relatively sudden intensity drop across a narrow temperature range, as they undergo the cooperative L_α to gel transition. One difference with the solvent molecules is that the lipid acyl chain signals also show a gradual, but notable, temperature-dependent intensity decrease before the phase transition. We attribute this to temperature-dependent changes in acyl chain fluidity within the motional regime that affects the NMR relaxation behavior. These motions are sensitive to the viscosity of the membrane core, which is dictated by lipid composition, presence of sterols, and the presence of double bonds. The temperature-dependence in the L_α phase is emphasized in saturated DMPC or partially saturated lipids (SOPC/POPC/OPPC), due to their increased viscosity compared with solvent molecules or lipids without saturated acyl chains (e.g., Fig. 2).

For each lipid, we determined the apparent T_m value by identifying the narrow temperature range over which the phase transition occurred, and then interpolating the halfway point. The resulting $T_{m,MAS}$ points are marked with dashed red lines in Fig. 3. As a reference point, the figure also shows the published T_m values for each lipid with vertical red solid lines in Fig. 3 (13). In the case of DMPC, we find a $T_{m,MAS}$ of 25°C (Fig. 3 *A*), which is close the T_m observed by DSC (23.9°C; data not shown). MAS NMR heating and cooling runs again yield very similar transition point temperatures (Fig. S3). Unlike DMPC, but similar to the DOPC/TOCL sample, the SOPC, POPC and OPPC MLVs all have $T_{m,MAS}$ values that are systematically lower than their normal T_m temperatures (Fig. 3, *B–D*). As listed in Table 1, SOPC, POPC, and OPPC have a T_m at 6.9°C, −2.5°C, and −8.9°C, respectively, in calorimetric measurements, but here have $T_{m,MAS}$ values of −4°C, −14°C, and −19°C, respectively.

DISCUSSION

Freezing of water under MAS NMR conditions

We previously reported the freezing point of water and the T_m of unilamellar lipid vesicles to be depressed in our MAS ssNMR studies of a peripherally bound protein (29). Here, a similar reduction in the freezing point of water was observed in MAS NMR studies of a variety of multilamellar lipid samples—both lipid mixtures and pure lipids. As shown in Figs. 2 and 3, the water freezing point was changed by as much as −25°C (SOPC MLVs; Fig. 3 *B*). A similar reduction in the water freezing temperature is commonly observed in MAS ssNMR studies of biological samples (42–45). For instance, MAS NMR studies on tightly packed protein crystals showed that the bulk water did not completely freeze until below −15°C, whereas crystal waters remained unfrozen until −25°C (42). One mechanism likely contributing to the observed freezing point reduction is a concentration-based effect, as is typically used to explain the dose-dependent effect of solutes on the freezing point of their solvent (46). Earlier studies have also discussed confinement effects, sometimes also referred to as capillary effects (42,47,48). In confined spaces the

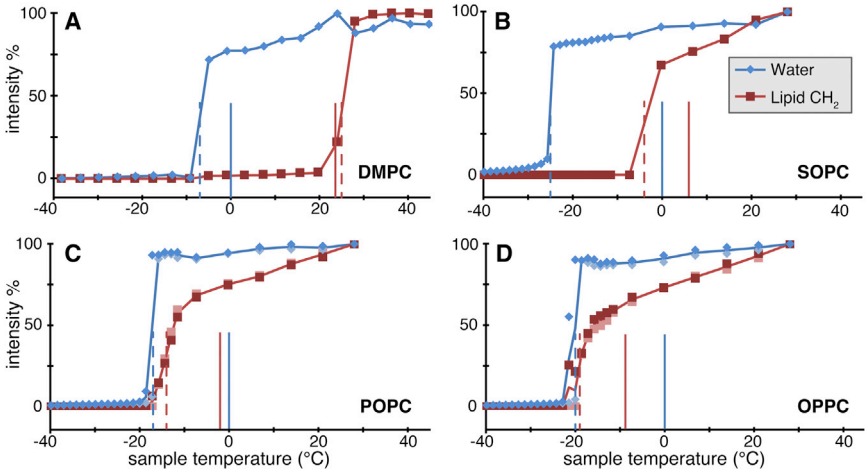

FIGURE 3 Intensity of ^{1}H MAS ssNMR peaks of water (*diamonds*) and lipid CH_2 groups (*squares*) as a function of sample temperature. These peak heights correlate to the dynamics of the solvent and lipid core, respectively. Data are shown for MLVs of (*A*) DPMC, (*B*) SOPC, (*C*) POPC, and (*D*) OPPC. For both water and lipid, the midpoint of the phase transition ($T_{m,MAS}$) is marked with dashed vertical lines. Solid vertical lines show the normal T_m (*red*), and 0°C (*blue*). To see this figure in color, go online.

freezing point of water is very much dependent on the heterogeneous nucleation of water (47), causing, e.g., small water droplets to have a much lower freezing point (40,41). MAS ssNMR sample holders (rotors) have μL-sized internal sample volumes: ~35 μL for the 3.2 mm (outer diameter) rotors employed in this study. More importantly, protocols for preparing MAS ssNMR samples typically maximize signal-to-noise by densely packing the (nonaqueous) material of interest: lipids, proteins, or other (bio)materials. In our studies (29–31,45,49), this is routinely accomplished by pelleting membrane or fibril samples in an ultracentrifuge. In the resulting sample, the amount of "bulk" water is purposely minimized, while (even transient) sample dehydration is reliably avoided.

In the resulting samples of tightly pelleted LUVs, the total water content constitutes ~77% of the total sample mass (29). In MLVs there is little bulk water, with most of the water being either within, or associated with, MLV PC vesicles (50). To gain an appreciation of the different water pools in densely packed lipid vesicle samples, we constructed a simplified schematic model assuming hard-sphere optimal packing of spherical vesicles. This model is illustrated in Fig. 4. The vesicle spheres have a diameter of 200 nm and a 5 nm total bilayer thickness. The figure also shows the ~25 Å hydration water layer that is associated with the lipid bilayers (51). The different types of water pools are indicated: intravesicular water, membrane-associated hydration water, and intervesicle water pockets. The latter pool has also been described as "lake water" in previous work (52). Using this highly schematic model, we calculated the expected relative sizes of the different water pools within the packed pellet (Fig. 4 *B*, *inset*). Most water (64%) is within the vesicles, and 26% is in the intervesicle spaces. In "real" samples the latter number may be smaller due to the ability of the vesicles to deform during sample packing. None of these water pools have length scales exceeding 200 nm, resulting in a confinement that lowers the water freezing point. This effect is not constrained to MAS NMR samples, as earlier non-NMR work also reports nonbulk (e.g., interlamellar and internal) water in phospholipid preparations to experience large reductions in its freezing point (6,53).

Lowering of the lipid melting temperatures

Although the changes in the freezing point of the hydration water were in line with previous reports on other types of MAS ssNMR samples, we also found a surprising lowering of the T_m of a variety of lipid types and mixtures. Aside from our recent report (29), we are not aware of previous MAS NMR studies of this particular phenomenon. We find a large reduction (by more than 10°C) of the T_m of lipids with freezing points that are normally close to, or below, the freezing point of water. In contrast DMPC, which has a T_m near room temperature, showed a much smaller change in its phase behavior. The T_m reduction affects both LUVs and MLVs, in presence and absence of bound protein, and both in pure lipids and mixed lipid vesicles (29). Thus, this effect appears to be generally applicable to the hydrated lipid bilayers found in these MAS ssNMR samples.

At first glance, there is an apparent analogy between the reductions in the T_m of water and that of the lipid bilayers. Although this may suggest an analogous molecular origin, it is unlikely that similar confinement effects can explain the changed lipid T_m values. Unlike the solvent molecules, the lipid acyl chains are not present in true three-dimensional "bulk" phase, but are instead constrained to the pseudo-two-dimensional lipid bilayer plane. Then, the primary variable in the geometry of lipid vesicles of a certain composition relates to the in-plane bilayer area (i.e., the surface area of spherical vesicles). Neither previous studies, nor our data, show a strong correlation between this parameter and the observed T_m value, at least in the regime of MLVs and LUVs that we studied. We observe a similar T_m depression in both MLVs and LUVs (29). Previous work also notes that MLVs and LUVs have very similar T_m values (13,14). Thus, the confinement-induced effect

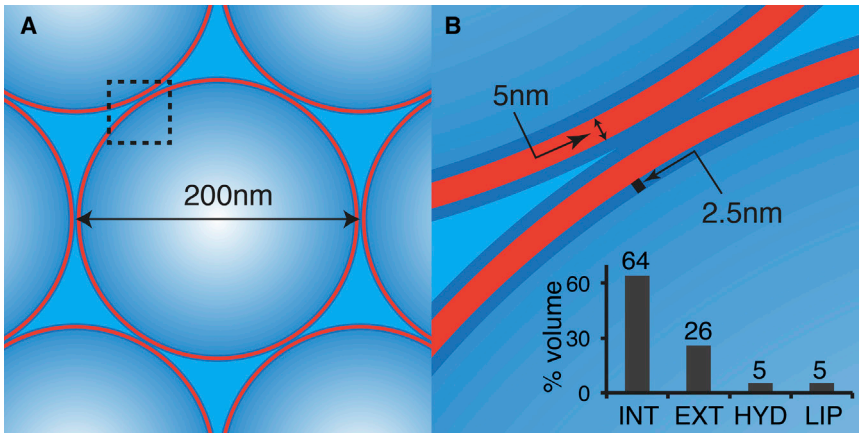

FIGURE 4 Schematic model of the geometry of densely packed LUVs. (*A*) Hexagonal dense packing of hard-sphere LUVs with a 200 nm diameter is shown. (*B*) Enlargement of the boxed area from (*A*) is provided. Dimensions of the bilayer (5 nm) and associated hydration water (2.5 nm) are indicated. The bar graph indicates the volumetric breakdown of water inside the LUVs (INT), between vesicles (EXT), hydration water layers (HYD), and the lipids themselves (LIP). To see this figure in color, go online.

does not apply to the lipid phase transition. What is then the cause of the T_m change?

On the potential role of centrifugal forces due to MAS

There are a few experimental parameters that are modulated by the use of MAS, and that conceivably could affect the lipid phase behavior. The centrifugal force caused by MAS can lead to increases in the local pressure and cause dehydration of the lipid bilayers. Both these parameters are known to affect lipids' gel-to-liquid crystalline transitions. Previous studies (54,55) report that increased pressure causes a shift of the T_m toward higher temperatures. In contrast, we observe a change of T_m toward lower temperatures. We also performed variable temperature measurements on OPPC MLVs at reduced MAS rates of 1 and 5 kHz, with little effect on the detected T_m values (data not shown). Thus, the lowering of the lipid T_m values is not due to increased pressures under MAS.

Centrifugal forces associated with (fast) MAS can also lead to partial dehydration of the lipid headgroups (56). Might this contribute to the observed lowering of T_m values? First, the dehydration of lipid bilayers is generally only observed at MAS rates well above 10 kHz, whereas all data in this study were obtained at 8.33 kHz or below. Second, dehydration favors the formation the gel phase, as it features fewer water molecules per lipid (57–61). Indeed, it is well known that dehydration of membranes (and cells) causes a dramatic *increase* in the lipids' T_m, rather than a decrease. Thus, not only is significant lipid dehydration unlikely under the employed conditions, but it would also cause the T_m to change in the opposite direction. Thus, we conclude that the MAS per se is not causing the lipid T_m depression.

Connection between lipid T_m and lowering of water's freezing point

We propose that the T_m change of the lipids is an indirect consequence of the freezing point depression of water. Ice formation, gel phase transitions, and membrane dehydration are connected processes (6). Ice formation in a confined pool of water depends on the volume of the water pool, with small volumes or droplets showing dramatically lower freezing points (47). As a consequence, ice formation happens first in the extravesicular bulk water, well before the intravesicular or interlamellar water pools freeze. This is analogous to the bulk and protein-associated water pools in crystalline and fibrillar protein samples (42–45). For lipid vesicles or cellular preparations, the formation of extravesicular (or extracellular) ice leads to both a dehydration and a disruption of the lipid bilayer. Dehydration of membranes favors gel formation, and thus causes a dramatic increase in the T_m. Indeed, it is thought that dehydration-induced gel phase formation plays a key role in freezing-induced damage to cells and cellular membranes (6). As the ice formation happens at much lower temperatures in our samples, the gel-phase-favoring membrane dehydration, which results from the ice formation, does not occur until lower temperatures. Thus, a lower lipid T_m may be achieved if one delays the dehydration effect that accompanies the (normally occurring) ice formation. There may also be another mechanism that takes effect in the absence of ice formation. When the solvent freezes, the lipid headgroup mobility is measurably reduced (29). The reduced mobility of the headgroups could limit the mobility of the attached acyl chains, which may also favor the gel transition. Lowering of the freezing point of the solvent can delay the gel-phase-transition through one or both of these processes reflecting an indirect coupling of solvent and acyl chain dynamics. Additional insights into their respective contributions may be available via simulation studies (61–63).

Implications

These observations have a number of practical and theoretical implications. First, they enhance our understanding of the fundamental underpinnings of lipid phase behavior, and in particular point to a role for solvent dynamics. The connections between ice formation and cell membrane integrity are also important in ongoing studies of freezing-tolerant organisms and other aspects of cryobiology. A number of previous studies have reported that cryoprotectants, such as trehalose, prevent dehydration-induced T_m increases (64–67). An interesting aspect of our study is that the freezing point depression was achieved without involvement of direct cryoprotectant-lipid interactions (68). The obtained results are also of interest for their implications for variable temperature studies of membrane-bound proteins and peptides, as well as whole cells, by MAS ssNMR. This notably includes the ongoing efforts to apply low-temperature dynamic nuclear polarization (DNP) to membrane-embedded proteins and whole cells (69,70).

CONCLUSION

We have examined in detail the melting point suppression of aqueous solvent and hydrated lipid bilayers. The solvent's melting point suppression generally affects biomolecular applications of ssNMR, not only to membranes and membrane-associated proteins, but also other kinds of densely packed biological solids. In addition, the surprising impact on the T_m of lipid-based biomembranes enhances our understanding of lipid phase behavior, and may have practical implications ranging from cryobiology to the use of cryoprotectants in the freezing and lyophilization of cells and lipid-based drug-delivery systems (71).

SUPPORTING MATERIAL

Three figures are available at http://www.biophysj.org/biophysj/supplemental/S0006-3495(16)30828-1.

AUTHOR CONTRIBUTIONS

A.M. made samples and performed experiments; A.M. and P.v.d.W. designed research, analyzed data, and wrote the manuscript.

ACKNOWLEDGMENTS

We thank Joel Gillespie at the Materials Characterization Lab for help with, and training for, the DSC measurements, and thank Mike Delk for help with the NMR instrumentation.

Funding support was from the University of Pittsburgh and the National Institutes of Health grant R01 GM113908.

SUPPORTING CITATIONS

References (72,73) appear in the Supporting Material.

REFERENCES

1. Van den Brink-van der Laan, E., J. A. Killian, and B. de Kruijff. 2004. Nonbilayer lipids affect peripheral and integral membrane proteins via changes in the lateral pressure profile. *Biochim. Biophys. Acta.* 1666:275–288.
2. Marsh, D. 2007. Lateral pressure profile, spontaneous curvature frustration, and the incorporation and conformation of proteins in membranes. *Biophys. J.* 93:3884–3899.
3. Zhou, H.-X., and T. A. Cross. 2013. Influences of membrane mimetic environments on membrane protein structures. *Annu. Rev. Biophys.* 42:361–392.
4. Laganowsky, A., E. Reading, …, C. V. Robinson. 2014. Membrane proteins bind lipids selectively to modulate their structure and function. *Nature.* 510:172–175.
5. Nagle, J. F., and S. Tristram-Nagle. 2000. Structure of lipid bilayers. *Biochim. Biophys. Acta.* 1469:159–195.
6. Wolfe, J., and G. Bryant. 1999. Freezing, drying, and/or vitrification of membrane-solute-water systems. *Cryobiology.* 39:103–129.
7. de Kruijff, B. 1997. Lipid polymorphism and biomembrane function. *Curr. Opin. Chem. Biol.* 1:564–569.
8. Aibara, S., M. Kato, …, M. Kito. 1972. Changes in positional distribution of fatty acids in the phospholipids of Escherichia coli after shift-down in temperature. *Biochim. Biophys. Acta.* 270:301–306.
9. Weerkamp, A., and W. Heinen. 1972. Effect of temperature on the fatty acid composition of the extreme thermophiles, Bacillus caldolyticus and Bacillus caldotenax. *J. Bacteriol.* 109:443–446.
10. van der Wel, P. C. A., T. Pott, …, J. A. Killian. 2000. Tryptophan-anchored transmembrane peptides promote formation of nonlamellar phases in phosphatidylethanolamine model membranes in a mismatch-dependent manner. *Biochemistry.* 39:3124–3133.
11. Eddy, M. T., T.-C. Ong, …, R. G. Griffin. 2012. Lipid dynamics and protein-lipid interactions in 2D crystals formed with the β-barrel integral membrane protein VDAC1. *J. Am. Chem. Soc.* 134:6375–6387.
12. Huang, C. H. 2001. Mixed-chain phospholipids: structures and chain-melting behavior. *Lipids.* 36:1077–1097.
13. Koynova, R., and M. Caffrey. 1998. Phases and phase transitions of the phosphatidylcholines. *Biochim. Biophys. Acta.* 1376:91–145.
14. Silvius, J. R. 1982. Thermotropic phase transitions of pure lipids in model membranes and their modifications by membrane proteins. *In* Lipid-Protein Interactions. John Wiley, New York.
15. Fenske, D. B., and P. R. Cullis. 2007. Lipid polymorphism. *In* Encyclopedia of Magnetic Resonance. John Wiley, Chichester, UK.
16. Nowacka, A., P. C. Mohr, …, D. Topgaard. 2010. Polarization transfer solid-state NMR for studying surfactant phase behavior. *Langmuir.* 26:16848–16856.
17. Van der Wel, P. C. A. 2014. Lipid dynamics and protein-lipid interactions in integral membrane proteins: insights from solid-state NMR. *eMagRes.* 3:111–118.
18. Dufourc, E. J., C. Mayer, …, G. Kothe. 1992. Dynamics of phosphate head groups in biomembranes. Comprehensive analysis using phosphorus-31 nuclear magnetic resonance lineshape and relaxation time measurements. *Biophys. J.* 61:42–57.
19. Gross, J. D., D. E. Warschawski, and R. G. Griffin. 1997. Dipolar recoupling in MAS NMR: a probe for segmental order in lipid bilayers. *J. Am. Chem. Soc.* 119:796–802.
20. Forbes, J., C. Husted, and E. Oldfield. 1988. High-field, high-resolution proton magic-angle sample-spinning nuclear magnetic resonance spectroscopic studies of gel and liquid crystalline lipid bilayers and the effects of cholesterol. *J. Am. Chem. Soc.* 110:1059–1065.
21. Polozov, I. V., and K. Gawrisch. 2006. Characterization of the liquid-ordered state by proton MAS NMR. *Biophys. J.* 90:2051–2061.
22. Holland, G. P., and T. M. Alam. 2006. Multi-dimensional ^{1}H-^{13}C HETCOR and FSLG-HETCOR NMR study of sphingomyelin bilayers containing cholesterol in the gel and liquid crystalline states. *J. Magn. Reson.* 181:316–326.
23. Purusottam, R. N., L. Sénicourt, …, P. Tekely. 2015. Probing the gel to liquid-crystalline phase transition and relevant conformation changes in liposomes by 13C magic-angle spinning NMR spectroscopy. *Biochim. Biophys. Acta.* 1848:3134–3139.
24. Hong, M., Y. Zhang, and F. Hu. 2012. Membrane protein structure and dynamics from NMR spectroscopy. *Annu. Rev. Phys. Chem.* 63:1–24.
25. Baker, L. A., and M. Baldus. 2014. Characterization of membrane protein function by solid-state NMR spectroscopy. *Curr. Opin. Struct. Biol.* 27:48–55.
26. Wang, T., S. D. Cady, and M. Hong. 2012. NMR determination of protein partitioning into membrane domains with different curvatures and application to the influenza M2 peptide. *Biophys. J.* 102:787–794.
27. Tang, M., A. J. Waring, and M. Hong. 2009. Effects of arginine density on the membrane-bound structure of a cationic antimicrobial peptide from solid-state NMR. *Biochim. Biophys. Acta.* 1788:514–521.
28. Banigan, J. R., A. Gayen, and N. J. Traaseth. 2014. Correlating lipid bilayer fluidity with sensitivity and resolution of polytopic membrane protein spectra by solid-state NMR spectroscopy. *Biochim. Biophys. Acta.* 1848:334–341.
29. Mandal, A., C. L. Hoop, …, P. C. A. van der Wel. 2015. Structural changes and proapoptotic peroxidase activity of cardiolipin-bound mitochondrial cytochrome c. *Biophys. J.* 109:1873–1884.
30. Li, J., C. L. Hoop, …, P. C. A. van der Wel. 2011. Amyloid-like fibrils from a domain-swapping protein feature a parallel, in-register conformation without native-like interactions. *J. Biol. Chem.* 286:28988–28995.
31. Hoop, C. L., V. N. Sivanandam, …, P. C. A. van der Wel. 2012. Structural characterization of the caveolin scaffolding domain in association with cholesterol-rich membranes. *Biochemistry.* 51:90–99.
32. Bertini, I., F. Engelke, …, E. Ravera. 2012. On the use of ultracentrifugal devices for sedimented solute NMR. *J. Biomol. NMR.* 54:123–127.
33. Thurber, K. R., and R. Tycko. 2009. Measurement of sample temperatures under magic-angle spinning from the chemical shift and spin-lattice relaxation rate of ^{79}Br in KBr powder. *J. Magn. Reson.* 196:84–87.
34. Sarkar, R., M. Concistrè, …, M. H. Levitt. 2011. An NMR thermometer for cryogenic magic-angle spinning NMR: the spin-lattice relaxation of (127)I in cesium iodide. *J. Magn. Reson.* 212:460–463.
35. Cavanagh, J., W. J. Fairbrother, …, N. J. Skleton. 2007. Protein NMR Spectroscopy: Principles and Practice. Academic Press, Burlington, MA.

36. Dvinskikh, S. V., V. Castro, and D. Sandström. 2004. Heating caused by radiofrequency irradiation and sample rotation in ^{13}C magic angle spinning NMR studies of lipid membranes. *Magn. Reson. Chem.* 42:875–881.

37. Delaglio, F., S. Grzesiek, …, A. Bax. 1995. NMRPipe: a multidimensional spectral processing system based on UNIX pipes. *J. Biomol. NMR.* 6:277–293.

38. Vranken, W. F., W. Boucher, …, E. D. Laue. 2005. The CCPN data model for NMR spectroscopy: development of a software pipeline. *Proteins.* 59:687–696.

39. Stevens, T. J., R. H. Fogh, …, E. D. Laue. 2011. A software framework for analysing solid-state MAS NMR data. *J. Biomol. NMR.* 51 :437–447.

40. Tsukahara, T., A. Hibara, …, T. Kitamori. 2007. NMR study of water molecules confined in extended nanospaces. *Angew. Chem. Int. Ed. Engl.* 46:1180–1183.

41. Hansen, E. W., M. Stöcker, and R. Schmidt. 1996. Low-temperature phase transition of water confined in mesopores probed by NMR. Influence on pore size distribution. *J. Phys. Chem.* 100:2195–2200.

42. Böckmann, A., C. Gardiennet, …, A. Lesage. 2009. Characterization of different water pools in solid-state NMR protein samples. *J. Biomol. NMR.* 45:319–327.

43. Lewandowski, J. R., M. E. Halse, …, L. Emsley. 2015. Protein dynamics. Direct observation of hierarchical protein dynamics. *Science.* 348:578–581.

44. Kloepper, K. D., D. H. Zhou, …, C. M. Rienstra. 2007. Temperature-dependent sensitivity enhancement of solid-state NMR spectra of alpha-synuclein fibrils. *J. Biomol. NMR.* 39:197–211.

45. Hoop, C. L., H.-K. Lin, …, P. C. A. van der Wel. 2014. Polyglutamine amyloid core boundaries and flanking domain dynamics in huntingtin fragment fibrils determined by solid-state nuclear magnetic resonance. *Biochemistry.* 53:6653–6666.

46. Koschke, K., H. J. Limbach, …, D. Donadio. 2015. Freezing point depression in model Lennard-Jones solutions. *Mol. Phys.* 113:2725–2734.

47. Christenson, H. K. 2001. Confinement effects on freezing and melting. *J. Phys. Condens. Matter.* 13:R95–R133.

48. Szyperski, T., and J. L. Mills. 2011. NMR-based structural biology of proteins in supercooled water. *J. Struct. Funct. Genomics.* 12:1–7.

49. Hoop, C. L., H.-K. Lin, …, P. C. A. van der Wel. 2016. Huntingtin exon 1 fibrils feature an interdigitated β-hairpin-based polyglutamine core. *Proc. Natl. Acad. Sci. USA.* 113:1546–1551.

50. Doherty, T., and M. Hong. 2009. 2D ^{1}H-^{31}P solid-state NMR studies of the dependence of inter-bilayer water dynamics on lipid headgroup structure and membrane peptides. *J. Magn. Reson.* 196:39–47.

51. Rand, R. P., and V. A. Parsegian. 1989. Hydration forces between phospholipid-bilayers. *Biochim. Biophys. Acta.* 988:351–376.

52. Nagle, J. F., Y. Liu, …, R. E. Stark. 1999. Re-analysis of magic angle spinning nuclear magnetic resonance determination of interlamellar waters in lipid bilayer dispersions. *Biophys. J.* 77:2062–2065.

53. Gleeson, J. T., S. Erramilli, and S. M. Gruner. 1994. Freezing and melting water in lamellar structures. *Biophys. J.* 67:706–712.

54. Potekhin, S. A., A. A. Senin, …, R. S. Khusainova. 2008. High pressure effect on the main transition from the ripple gel P'_{β} phase to the liquid crystal (L_{α}) phase in dipalmitoylphosphatidylcholine. Microcalorimetric study. *Biochim. Biophys. Act.* 1778:2588–2593.

55. Tada, K., E. Miyazaki, …, S. Kaneshina. 2009. Barotropic and thermotropic bilayer phase behavior of positional isomers of unsaturated mixed-chain phosphatidylcholines. *Biochim. Biophys. Act.* 1788: 1056–1063.

56. Gawrisch, K., and H. C. Gaede. 2007. Measurement of lateral diffusion rates in membranes by pulsed magnetic field gradient, magic angle spinning-proton nuclear magnetic resonance. *In* Methods in Membrane Lipids. A. M. Dopico, editor. Humana Press, Totowa, NJ, pp. 257–265.

57. Janiak, M. J., D. M. Small, and G. G. Shipley. 1979. Temperature and compositional dependence of the structure of hydrated dimyristoyl lecithin. *J. Biol. Chem.* 254:6068–6078.

58. Smith, G. S., E. B. Sirota, …, N. A. Clark. 1988. Structure of the L beta phases in a hydrated phosphatidylcholine multimembrane. *Phys. Rev. Lett.* 60:813–816.

59. Faure, C., L. Bonakdar, and E. J. Dufourc. 1997. Determination of DMPC hydration in the $L(\alpha)$ and $L(\beta')$ phases by ^{2}H solid state NMR of D_2O. *FEBS Lett.* 405:263–266.

60. Nowacka, A., S. Douezan, …, E. Sparr. 2012. Small polar molecules like glycerol and urea can preserve the fluidity of lipid bilayers under dry conditions. *Soft Matter.* 8:1482–1491.

61. Kowalik, B., T. Schubert, …, E. Schneck. 2015. Combination of MD simulations with two-state kinetic rate modeling elucidates the chain melting transition of phospholipid bilayers for different hydration levels. *J. Phys. Chem. B.* 119:14157–14167.

62. Knecht, V., A. E. Mark, and S.-J. Marrink. 2006. Phase behavior of a phospholipid/fatty acid/water mixture studied in atomic detail. *J. Am. Chem. Soc.* 128:2030–2034.

63. Coppock, P. S., and J. T. Kindt. 2010. Determination of phase transition temperatures for atomistic models of lipids from temperature-dependent stripe domain growth kinetics. *J. Phys. Chem. B.* 114:11468–11473.

64. Crowe, J. H., L. M. Crowe, …, T. J. Anchordoguy. 1988. Interactions of sugars with membranes. *Biochim. Biophys. Act.* 947:367–384.

65. Rudolph, A. S., J. H. Crowe, and L. M. Crowe. 1986. Effects of three stabilizing agents—proline, betaine, and trehalose—on membrane phospholipids. *Arch. Biochem. Biophys.* 245:134–143.

66. Green, J. L., and C. A. Angell. 1989. Phase relations and vitrification in saccharide-water solutions and the trehalose anomaly. *J. Phys. Chem.* 93:2880–2882.

67. Koster, K. L., Y. P. Lei, …, G. Bryant. 2000. Effects of vitrified and nonvitrified sugars on phosphatidylcholine fluid-to-gel phase transitions. *Biophys. J.* 78:1932–1946.

68. Moiset, G., C. A. López, …, S.-J. Marrink. 2014. Disaccharides impact the lateral organization of lipid membranes. *J. Am. Chem. Soc.* 136:16167–16175.

69. Renault, M., S. Pawsey, …, M. Baldus. 2012. Solid-state NMR spectroscopy on cellular preparations enhanced by dynamic nuclear polarization. *Angew. Chem. Int. Ed. Engl.* 51:2998–3001.

70. Kaplan, M., A. Cukkemane, …, M. Baldus. 2015. Probing a cell-embedded megadalton protein complex by DNP-supported solid-state NMR. *Nat. Methods.* 12:649–652.

71. Wissing, S. A., O. Kayser, and R. H. Müller. 2004. Solid lipid nanoparticles for parenteral drug delivery. *Adv. Drug Deliv. Rev.* 56:1257–1272.

72. Lewis, R. N. A. H., and R. N. McElhaney. 2009. The physicochemical properties of cardiolipin bilayers and cardiolipin-containing lipid membranes. *Biochim. Biophys. Acta.* 1788:2069–2079.

73. Boscia, A. L., B. W. Treece, …, S. Tristram-Nagle. 2014. X-ray structure, thermodynamics, elastic properties and MD simulations of cardiolipin/dimyristoylphosphatidylcholine mixed membranes. *Chem. Phys. Lipids.* 178:1–10.